

Dependence of potentiometric oxygen sensing characteristics on the nature of electrodes

Ramasamy Ramamoorthy, Sheikh A. Akbar, Prabir. K. Dutta *

Center for Industrial Sensors and Measurements (CISM), Department of Materials Science and Engineering,
2041 College Road, Ohio State University, Columbus, OH 43210-1178, USA

Received 11 January 2005; received in revised form 14 February 2005; accepted 18 February 2005
Available online 13 March 2005

Abstract

A comparative study of gas sensing response and electrical properties of three electrodes for a potentiometric YSZ-based oxygen sensor is presented. Platinum (Pt), lanthanum strontium iron cobalt oxide ($\text{La}_{0.6}\text{Sr}_{0.4}\text{Fe}_{0.8}\text{Co}_{0.2}\text{O}_3$: LSFCE) and chromium oxide (Cr_2O_3) were used as the sensing electrodes. The microstructural features, electrochemical impedance for the charge transfer processes and oxygen sensing characteristics were studied at different temperatures and correlated. Impedance measurements indicate that the LSFCE electrode exhibits lower resistance and higher capacitance by almost two to three orders of magnitude for the chemical exchange and ion transfer processes compared to the other two electrodes. The relaxation time constants of all three electrodes are comparable to each other and found to be in the range of fraction of a second. But, the measured response times for oxygen sensors using these electrodes showed values of the order of minutes at temperatures of 500 °C and below. So, the controlling factor for oxygen response at temperatures below 500 °C seems to be adsorption and/or surface diffusion of oxygen rather than the charge transfer process for a given morphology of the electrode.

© 2005 Elsevier B.V. All rights reserved.

Keywords: Oxygen sensor; Interfacial impedance; Triple phase boundaries; Sensing electrodes; Response time

1. Introduction

Development and optimization of electrodes is an important area of study for solid oxide fuel cell (SOFC) and chemical gas sensor applications [1–4]. Our interest is directed primarily on gas sensors and understanding why different oxide electrodes exhibit different sensitivities in mixed potential NO_x and CO sensors [5]. The output voltage of these sensors is determined by the mixed potentials generated from the oxygen and NO_x electrochemistry on the sensing electrode and depends upon the kinetics of oxygen reduction and transport at the electrode. Thus, understanding the kinetics of oxygen exchange reactions at the electrode interface is a necessary first step towards evaluation of the sensor behavior [6].

For devices based on oxygen ion conducting solid electrolytes, the reactions of oxygen at the electrode constitute diffusion through the porous electrode, redox reaction involving electron transfer ($1/2\text{O}_2 + 2e^- \leftrightarrow \text{O}^{2-}$), and the oxygen ion transfer from the electrode to the electrolyte. While the adsorption and charge/ion transfer processes are controlled by the catalytic and electrical properties of the electrodes, the diffusion of oxygen is dependent on the electrode microstructure. Amongst well-studied electrode systems are metal (e.g., platinum) electrodes and mixed ionic–electronic conducting (MIEC) electrodes (e.g., lanthanum strontium manganite: LSMO). In the case of metals, the charge transfer processes take place at the triple phase boundaries (TPB) between the electrode, electrolyte and the gas-phase. Steady state current–voltage polarization measurements on porous Pt–YSZ cell under varying p_{O_2} by Robertson and Michaels [7] indicate that due to low solubility and diffusivity of oxygen in bulk platinum, transport of oxygen through the bulk electrode is not feasible. So,

* Corresponding author. Address: Department of Chemistry, 120 W. 18th Avenue, Ohio State University, Columbus, OH 43210, USA.
Tel.: +1 614 2924532; fax: +1 614 688 5402.

E-mail address: dutta@chemistry.ohio-state.edu (Prabir.K. Dutta).

the only path for ionic transport is through the triple phase boundaries at the electrode–electrolyte interface. Also it is indicated that oxygen is supplied to the TPBs by surface diffusion of dissociatively adsorbed oxygen [7,8]. So, the effective reaction zone (ERZ) for the chemical exchange and ion transfer is restricted to the boundary around the periphery of the electrode particles on the electrolyte.

On the other hand, the mixed ionic–electronic conducting electrodes, e.g., LSMO, lanthanum strontium cobaltite (LSCO) and lanthanum strontium iron cobalt oxide (LSFCO) have extended reaction zone for the charge transfer processes from the TPBs to the electrode surface and bulk. As these perovskite-structured electrodes exhibit mixed ionic–electronic conductivity and high diffusion (D) and surface exchange (k) coefficients ($D = 2.2 \times 10^{-2} \mu\text{m}^2/\text{s}$, $k = 3.4 \times 10^{-3} \mu\text{m}/\text{s}$ at 600°C for LSFCO) [9], the chemical exchange reaction is more dominant at the electrode surface than at the TPBs [10]. So, the overall oxygen reaction kinetics is faster than that at the metallic electrodes and is manifested in the charge transfer resistance (R_{ct}) and the double layer capacitance (C_{dl}) of the electrode [11–14]. LSFCO is found to have the highest electrical conductivity among the La-based perovskite electrodes ($\sigma \approx 500 \text{ S/cm}$ at 600°C) [15] and the ionic conductivity is $5 \times 10^{-4} \text{ S/cm}$ [16] and hence it is considered to be one of the best electrode materials for electrochemical devices at intermediate temperatures ($<800^\circ\text{C}$) [17,18].

As many spinel compounds with chromium [4] and chromium oxide itself [5] exhibit significant sensitivity to NO_x gas, evaluation of the Cr_2O_3 electrode for oxygen exchange reactions is worth exploring. Cr_2O_3 is a p-type semiconductor with electronic conductivity of about $5 \times 10^{-3} \text{ S/cm}$ at 600°C and is independent of oxygen pressure changes [19]. The oxygen diffusion coefficient is of the order of $10^{-9} \mu\text{m}^2/\text{s}$ at 1100°C , which leads to poor oxygen ion conduction in Cr_2O_3 [19].

In the present study, three electrodes, platinum, a MIEC (LSFCO) and a semiconductor (Cr_2O_3), were chosen as sensing electrodes for a YSZ based oxygen sensor. Impedance spectroscopy and SEM were used along with the gas-sensing measurements at different temperatures to explore the characteristics of the electrodes that influence the sensing behavior.

2. Experimental

An oxygen sensor based on a YSZ tube, one end closed, was fabricated using three different sensing electrodes: Pt-colloid, LSFCO and Cr_2O_3 . Commercial Pt-ink was used for the common air-reference electrode at the inner side of the YSZ tube. Pt-colloid was prepared by using dipotassium tetrachloroplatinate, (poly)vinyl alcohol (PVA), NaOH and sodium borohydride in deionized water [20]. LSFCO paste was prepared by mixing $\text{La}_{0.6}\text{Sr}_{0.4}\text{Fe}_{0.8}\text{Co}_{0.2}\text{O}_3$ powder (supplied by SCI Inc., USA) with α -terpineol. Similarly,

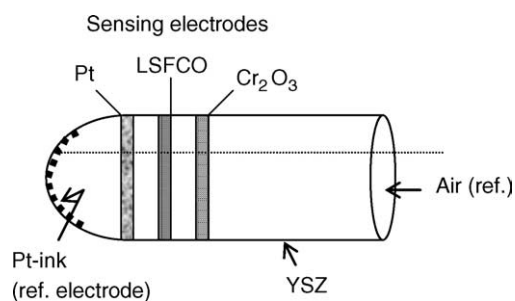


Fig. 1. Schematic diagram of the oxygen sensor cell with sensing electrodes. The YSZ tube dimensions are: 30 cm long and 8 mm diameter. The electrodes were pasted 3 mm wide ring.

a Cr_2O_3 (99%, Alfa Aesar) paste was prepared. The electrode pastes were applied sequentially in the order Pt-colloid, LSFCO and Cr_2O_3 from the closed end of the YSZ tube and fired at 1000°C for 1 h in air. The order of the electrode sequence was chosen arbitrarily. The schematic diagram of the sensor cell with different sensing electrodes on it is shown in Fig. 1. Platinum wires were attached to each electrode as connecting leads. Oxygen sensing measurements were carried out at 400, 500 and 600°C in different partial pressures of oxygen and the sensing response time for each electrode was estimated.

Impedance measurements were carried out on YSZ pellets with identical and symmetric electrodes on both sides. Y_2O_3 (8 mol%) stabilized ZrO_2 (8YSZ) pellets (from Tosoh powder, Japan) of 10 mm diameter and 1–2 mm thickness were used. Pt-colloid, LSFCO, Cr_2O_3 and commercial Pt pastes were applied on both sides of different YSZ pellets. Impedance measurements were performed on these cells at temperatures from 500 to 700°C in air (21% O_2), 10% and 3% O_2 in balance nitrogen in the frequency range of 1 MHz to 0.1 Hz with an ac amplitude of 10 mV. The gas flow was set at 100 cc/min for both sensing and impedance measurements. The electrode polarization resistance R (also called the charge transfer resistance) and the double layer capacitance or constant phase element (CPE) (Q) values were estimated by fitting the experimental data to the appropriate equivalent circuits consisting of R 's and Q 's. Since the electrodes are identical on both sides of the YSZ, the net resistance measured is twice that of the single interface and the capacitance is half the value of the single side electrode. The microstructure of the electrodes on the YSZ surface was studied by using SEM (Philips XL30).

3. Results

The experimental strategy was to examine the oxygen sensing characteristics of a YSZ based electrolyte with the three electrodes, Pt, LSFCO and Cr_2O_3 . Correlation of the sensing behavior with electrode microstructure and the electrochemistry at the electrode–electrolyte interface is developed with the help of electron microscopy and impedance spectroscopy.

3.1. Oxygen sensor response

The oxygen sensing characteristics of Pt-colloid, LSFCO and chromia electrodes on YSZ based potentiometric sensor were examined at 400, 500 and 600 °C. Fig. 2a compares the sensitivity for oxygen as a semi-logarithmic plot of the sensor output against oxygen partial pressure at 600 °C. With all three electrodes, a sensitivity of 43.4 mV/decade was observed, consistent with the prediction of the Nernst equation [21]. Fig. 2b shows the sensitivity plots of the electrodes at 500 °C. The chromia electrode showed a lower sensitivity (35.9 mV/decade) than the other electrodes (Pt-colloid and LSFCO). The corresponding values of the sensitivity for Pt and LSFCO electrodes is 38.8 mV/decade. The theoretical value for 500 °C is 38.3 mV/decade. At 400 °C (not shown here), the Pt and LSFCO electrodes showed equilibrium values of sensitivity while for the chromia electrode, equilibrium is not attained even after 10 min.

Fig. 3a compares the response transients of the sensing electrodes upon changing the p_{O_2} from 21% to 3% O_2 (in nitrogen) at 600 °C. The t_{90} response times, defined as the time to reach 90% of the steady state value, at 600 °C were found to be similar for all three electrodes with a value of 1 min. Fig. 3b shows the response transients at 500 °C. The t_{90} values at 500 °C were found to be 1.8, 1.1 and 3.2 min for Pt, LSFCO and Cr_2O_3 electrodes, respectively. At 400 °C, the response times increase to 5 min for Pt, 2 min for LSFCO and >10 min for Cr_2O_3 . Thus, the most significant change in

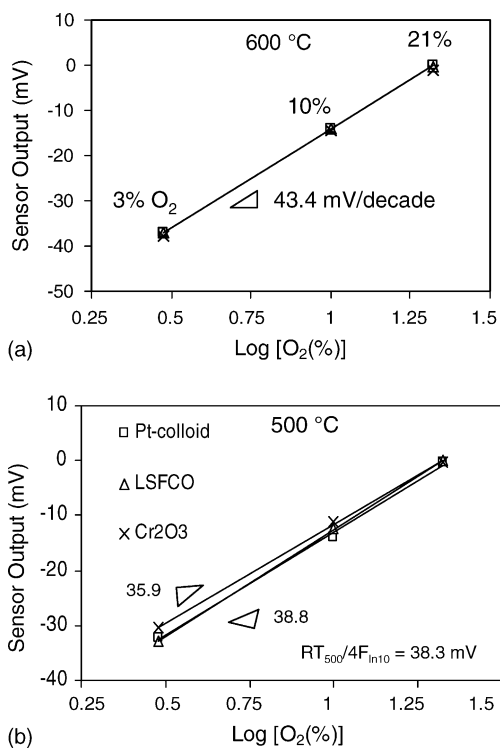


Fig. 2. Oxygen sensitivity characteristics of platinum, LSFCO and Cr_2O_3 electrodes at (a) 600 °C and (b) 500 °C.

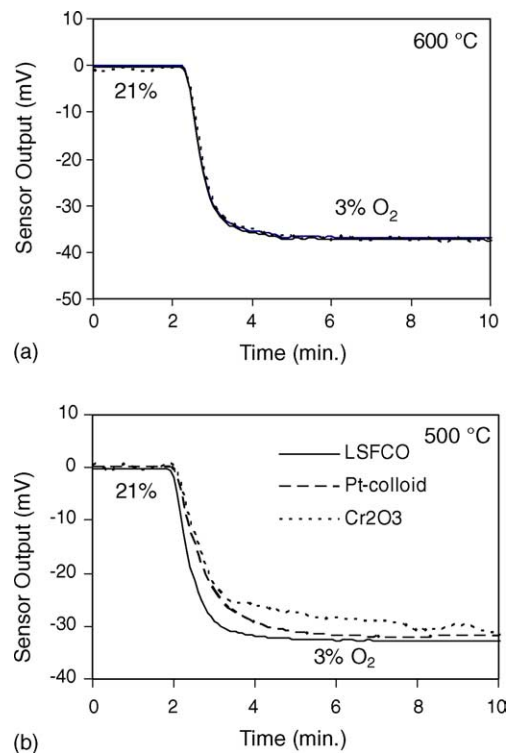


Fig. 3. Oxygen response characteristics of platinum, LSFCO and Cr_2O_3 electrodes at (a) 600 °C and (b) 500 °C upon changing O_2 from 21% to 3%. The response time includes the apparatus time as well.

the response time is observed with Cr_2O_3 , followed by Pt and LSFCO.

3.2. Electrode microstructure

The electrode pastes were applied on individual YSZ substrates for the SEM observations and processed the same way as for the sensing and electrical measurements. Fig. 4 shows the cross-sectional and top views of the Pt-colloid, LSFCO and Cr_2O_3 electrodes depicting the particle and porosity dispersion on YSZ. The colloidal platinum formed irregular aggregates of groundnut shaped small particles incorporating tiny pores within the aggregates themselves as shown in the inset of Fig. 4a. In the LSFCO electrode, a nearly homogeneous distribution of the particles and the porosity is observed throughout the sample as seen in Fig. 4b. On the other hand, the chromia electrode exhibits a relatively dense packing fraction of the particles (Fig. 4c).

3.3. Impedance spectroscopy

Impedance spectroscopy has been used to understand charge transfer mechanisms at electrode–electrolyte interfaces. In a typical impedance spectrum, the resistive and capacitive components of the bulk electrolyte and the electrode interface are identified by the frequency dispersion. The low frequency region represents the electrode polarization while the high frequency component represents electrolyte

impedance. For this study, the electrodes were placed symmetrically on both sides of the YSZ pellets. The impedance data were recorded at temperatures of 400–700 °C in 21% O₂ balance N₂. The impedance spectra with Pt, LSFCO and Cr₂O₃ electrodes at 600 °C are shown in Fig. 5a–c. All three electrodes show depressed semi-circles in the impedance plane. Similar data were obtained at 700 °C. At 500 °C, though the impedance spectra of the electrodes are incomplete in the given frequency range as shown in Fig. 6, the trends are similar to the observations at higher temperatures. The slightly flattened semi-circles corresponding to the Pt and Cr₂O₃ electrode impedance were fitted to a Randle circuit consisting of the electrolyte resistance R_b , the charge transfer resistance R and the constant phase element Q . The more flattened impedance semi-circle of the LSFCO electrode was

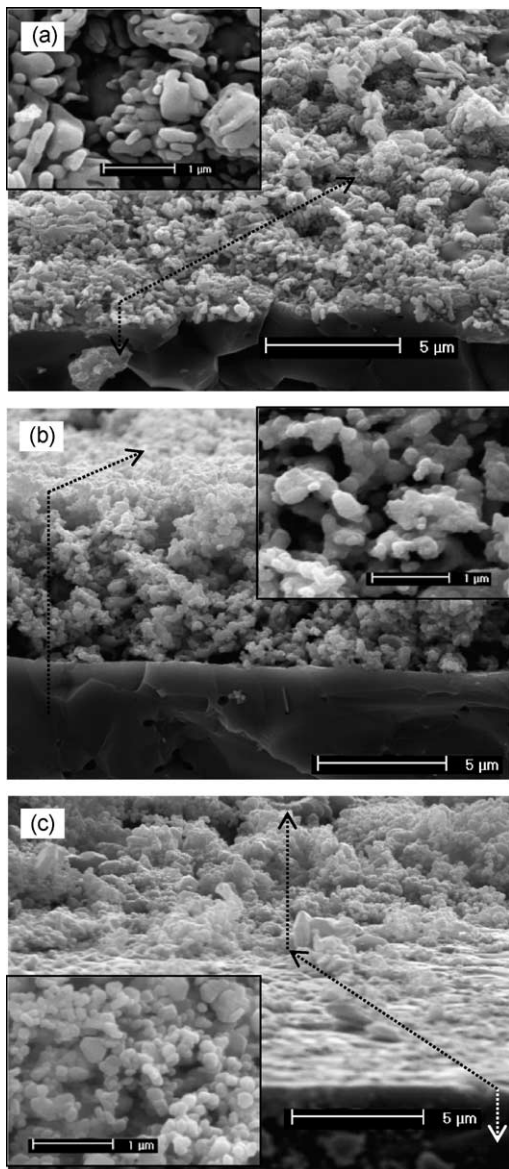


Fig. 4. Cross-sectional and top views (insets) of the electrode microstructures on YSZ: (a) Pt-colloid, (b) LSFCO and (c) Cr₂O₃.

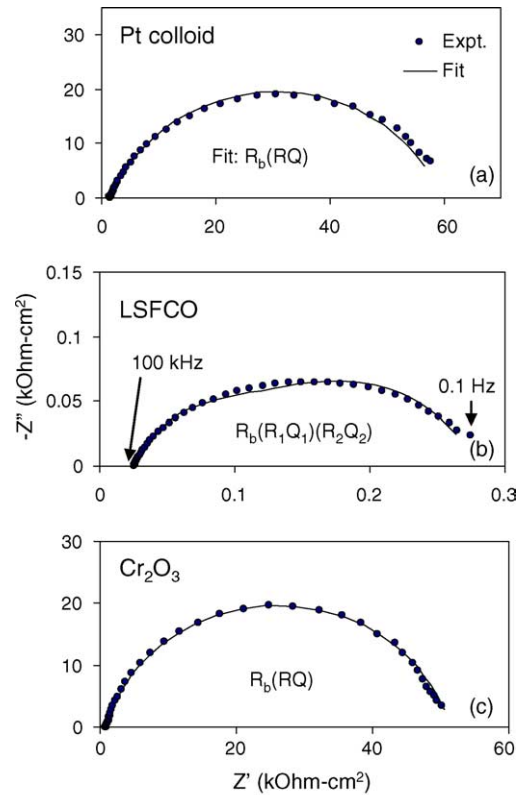


Fig. 5. Electrode Impedance spectra of (a) colloidal Pt, (b) LSFCO and (c) Cr₂O₃ electrodes with YSZ electrolyte at 600 °C in 21% O₂.

fitted with $R_b(R_1Q_1)(R_2Q_2)$, where the components in the parenthesis are connected in parallel. The constant phase element, Q can be represented by $k(j\omega)^{-n} = (k[\cos(n\pi/2) - j \sin(n\pi/2)]/\omega^n)$, where $j = \sqrt{-1}$, k and n are frequency independent parameters and $0 \leq n \leq 1$. When $n=0$, k represents an ideal resistor (i.e., $k=R$) and when $n=1$, it describes an ideal capacitor with $k=1/C$ (i.e., $Z_Q = 1/j\omega C$) [22].

The fitting parameters for all electrodes between 500 and 700 °C are shown in Table 1. At 500 °C, because of the incompleteness of the data in the low frequency region, the values of R and Q are not as precise. Some trends are evident. The resistance to oxygen reduction and transport at a particular temperature follows the order Cr₂O₃ > Pt ≫ LSFCO, whereas the apparent capacitance Q follows the order LS-

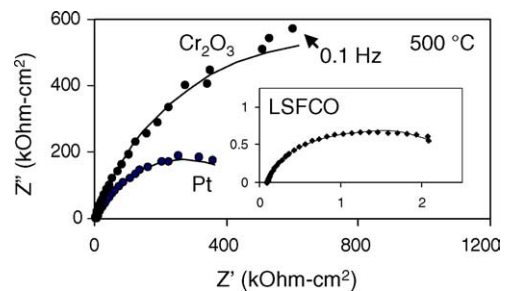


Fig. 6. Impedance spectra of Pt-colloid, chromia and LSFCO electrodes with YSZ electrolyte at 500 °C in air.

Table 1
The impedance parameters for Pt, Cr₂O₃ and LSFCO electrodes at 500, 600 and 700 °C

Electrode	<i>T</i> (°C)	<i>R</i> _{1(HF)} (Ω cm ²)	<i>Q</i> _{1(HF)} ^a (μF/cm ²)	<i>n</i> ₁	<i>R</i> _{2(LF)} (Ω cm ²)	<i>Q</i> _{2(LF)} ^a (μF/cm ²)	<i>n</i> ₂	<i>τ</i> ₁ (=R ₁ <i>Q</i> ₁) (s)	<i>τ</i> ₂ (=R ₂ <i>Q</i> ₂) (s)	<i>τ</i> _{net} (=R <i>Q</i>) (s)
Pt	500	5.25 × 10 ⁵	1.63	0.75	–	–	–	–	–	0.86
	600	5.83 × 10 ⁴	2.92	0.75	–	–	–	–	–	0.17
	700	5.3 × 10 ³	5.18	0.75	–	–	–	–	–	0.03
Cr ₂ O ₃	500	1.43 × 10 ⁶	1.02	0.80	–	–	–	–	–	1.45
	600	5.05 × 10 ⁴	1.17	0.84	–	–	–	–	–	0.06
	700	3.6 × 10 ³	1.88	0.82	–	–	–	–	–	0.007
LSFCO	500	759	126	0.82	1774	399	0.73	9.5 × 10 ⁻²	0.71	0.71
	600	81	152	0.82	170	838	0.75	1.2 × 10 ⁻²	0.14	0.14
	700	4	74	1.0	30	1210	0.65	3 × 10 ⁻⁴	0.04	0.04

*R*₁ and *Q*₁ and *R*₂ and *Q*₂ are derived from high and low frequency components, respectively, of the impedance fit in the case of LSFCO electrode.

^a The constant phase elements *Q*'s are approximated to capacitance for calculation of time constants ($\tau = RC$).

FCO \gg Pt > Cr₂O₃. *R* tends to decrease by about one to two orders of magnitude for every 100 °C increase in temperature, whereas *Q* shows an increase of a factor of 2–4 over the 500–700 °C range (except for the low frequency component of LSFCO at 700 °C). The value of '*n*' varies from 0.65 to 1. A value close to 1 can be regarded as the CPE being more capacitive and thus the unit of *Q* is taken as Farad for simplicity. Table 1 also lists the product R*Q*, which is a measure of the relaxation time ($\approx RC$) for the oxygen reduction and transport process. From the Arrhenius plots of the net resistances of the electrodes in Fig. 7, activation energies were calculated to be 1.7 eV for the Pt electrode, 1.2 eV for the LSFCO and 2 eV for chromia.

4. Discussion

Impedance spectroscopy provides information regarding the resistance and capacitance associated with an electrochemical process. In the present study, the resistance provides information regarding oxygen transport, reduction and ionic transfer at the electrode–electrolyte interface, whereas the constant phase element, *Q* is a measure of the capacitance, which arises due to build-up of O²⁻ ions. Increased redox processes lead to charging of the double layer and a large ap-

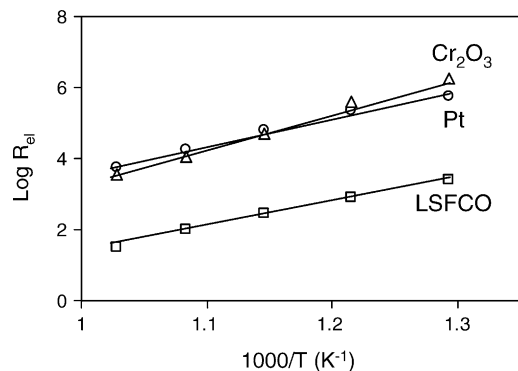


Fig. 7. Arrhenius plots of electrode resistance for the three electrodes.

parent capacitance. A large capacitance combined with the charge transfer resistance of the electrode results in a larger time constant of the oxygen exchange and transfer process. Warburton et al. [23] have observed a direct correlation between the *RC* time constants of the electrochemical process and the response time of the amperometric sensors.

In Pt and Cr₂O₃ electrodes, the cumulative values of resistance and capacitance derived from the single relaxation fit of the impedance data represent the processes involved with oxygen reduction and ion transfer at the TPBs. In the case of LSFCO, the impedance spectra could be separated into two relaxation processes: a high frequency process assigned to ionic transfer at the electrode–YSZ interface and a lower frequency process that involves transport and diffusion of oxygen through the electrode bulk [10,14,17]. The higher values of *R* in Pt and Cr₂O₃ as compared to LSFCO (Table 1) are a reflection of the fact that the charge transfer process occurs only at the triple phase boundaries, since the surface diffusion of oxygen is the only mode of mass transport in the Pt and Cr₂O₃ electrodes. Thus, the cumulative effects of adsorption, surface diffusion, chemical exchange and ion transfer processes lead to high values of electrode resistance for Pt and Cr₂O₃ electrodes though distinct relaxation process corresponding to the gas phase adsorption or diffusion is not observed in the impedance spectra at this temperature range. The activation energy for the charge transfer process measured by the dependence of *R* on temperature is also higher for Pt and Cr₂O₃, 1.7 eV and 2 eV, respectively, as compared to 1.2 eV for LSFCO. Previous studies on Pt/YSZ have reported activation energy of 2.06 eV for the charge transfer process [24]. The higher activation energy in Cr₂O₃ is comparable with the \sim 2.4 eV activation energy for oxygen diffusion in Cr₂O₃ [18]. Electronic conductivity of Cr₂O₃ has an activation energy of 0.6 eV and is not the limiting factor [25].

On the other hand, in LSFCO, due to its better catalytic and ionic conducting properties, the mass transport of adsorbed oxygen takes place via the electrode surface and bulk to reach the electrode–electrolyte interface. The increased

effective reaction zone throughout the electrode as opposed to just the TPB region in the Pt and Cr_2O_3 electrodes make the LSFCO less resistive to the electrochemical oxygen reactions which is demonstrated by the values given in Table 1. Since the oxygen transport is influenced mainly by the electrode bulk rather than the triple phase boundaries, the activation energy of 1.2 eV calculated from the net resistance is the characteristic of the electrode itself. Previous studies on LSFCO/YSZ have noted activation energies for oxygen reduction to be between 1.4 and 1.6 eV [18]. For LSFCO/CGO (cerium gadolinium oxide), activation energies of 1.5–1.6 eV and 1.2 eV have been reported [9,26].

Even though the overall resistance to oxygen transport and charge transfer in LSFCO at all temperatures is two to three orders of magnitude lower than Pt and Cr_2O_3 , the relaxation times for LSFCO (RQ) are comparable to Pt and Cr_2O_3 electrodes (Table 1), primarily due to the high values of capacitance in LSFCO. While the double layer capacitance represented by the constant phase element Q is of the order of a few $\mu\text{F}/\text{cm}^2$ in Pt and Cr_2O_3 electrodes, a characteristic of electrode capacitance, LSFCO exhibits hundreds of $\mu\text{F}/\text{cm}^2$ at all temperatures (Table 1). For LSFCO/YSZ, a previous study has noted capacitance of $1.16 \times 10^{-2} \text{ F}/\text{cm}^2$ [18] whereas for LSFCO/CGO, capacitance of $10^{-4} \text{ F}/\text{cm}^2$ and 10–20 $\mu\text{F}/\text{cm}^2$ have been reported [26,27]. When an external potential is applied at low frequency to a mixed ionic–electronic conductor, ions periodically accumulate at one side of the sample while becoming depleted at the other. In this situation, a mass transport with vanishing net current flow in the form of oxygen ions and electrons together takes place [28]. This is referred to as the chemical diffusion of oxygen, leading to the large apparent capacitance. Given this information on the impedance parameters of the three electrodes, it is now worth comparing the observed sensor response at different temperatures.

At 600 °C, the sensitivity and response time of the three electrodes are found to be similar. While the sensitivity is a true representation of the electrode behavior, the measured response time is determined by the combined effect of the electrode kinetics and the geometry of the measuring cell. The large volume of the measuring cell ($\sim 400 \text{ cm}^3$), the slow flow rate ($100 \text{ cm}^3/\text{min}$) of the gas stream and the intrinsic delay of gas mixing lead to an instrument response time. Any event that is happening on a faster time scale than the instrument response time will not be manifested. So, the fact that all three electrodes show the same response time of 1 min at 600 °C is a reflection of the instrument response time. At 500 °C and below, for the same gas flow conditions (as that of 600 °C), differences are observed in the response times, e.g., the t_{90} values are 1.8, 1.1 and 3.2 min in Pt, LSFCO and Cr_2O_3 electrodes, respectively. The measured t_{90} values of the electrodes being of the order of minutes at 500 °C and below are significantly higher than the RQ time constants. It seems that apart from the chemical exchange and ion transfer process, probably there is a non-electrical factor contributing to the response time at lower temperatures. As discussed ear-

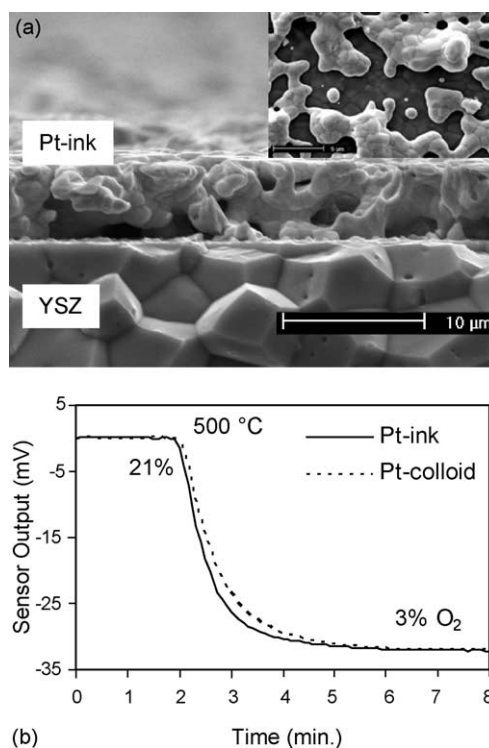


Fig. 8. The microstructure and the oxygen response transient at 500 °C of the commercial platinum ink electrode on YSZ.

lier, in LSFCO oxygen transport can occur through the bulk, whereas in Pt and Cr_2O_3 , surface diffusion of oxygen is the primary mechanism. Thus, with the latter electrodes, the microstructure should have an important effect on the response times, especially at lower temperatures. As shown in Fig. 4, all three electrodes exhibit a relatively dense packed fraction of the particles. Such microstructures may impede the diffusional motion of oxygen adsorbates along the pores and the particle surfaces. However, it is believed that the mass transport process is not fully represented in the measured RQ time constant which is mainly attributed to the charge transfer process though diffusion effects can be identified by measuring the electrode impedance at temperatures above 1000 °C [29].

If this hypothesis has merit, then altering the diffusion resistance by engineering the microstructure of the electrode should produce differences in the response times. This was done for Pt using commercial platinum ink as the electrode, which has a bismuth based impurity to help form refined microstructure and better bonding to the YSZ. Fig. 8a shows the morphology of the electrode, which is considerably more open, the triple phase boundaries are well defined, and easily accessible to the oxygen species compared to the Pt-colloid electrode. The response transients of the two Pt electrodes at 500 °C are compared in Fig. 8b and it is found that the electrode with the commercial Pt ink shows a faster response (1.4 min).

5. Conclusions

The oxygen sensing performance of Pt, LSFCO and Cr_2O_3 electrodes on the YSZ electrolyte at different temperatures was analyzed. Significant differences were observed in both the sensitivity and response times of these electrodes, especially at and below 500°C . Impedance measurements suggest that the electrode resistance to oxygen reduction and ion transfer at temperatures 600°C and below follows the order $\text{Cr}_2\text{O}_3 > \text{Pt} \gg \text{LSFCO}$ and above 600°C $\text{Pt} > \text{Cr}_2\text{O}_3 \gg \text{LSFCO}$. The apparent capacitance of these electrodes follows the order $\text{LSFCO} \gg \text{Pt} > \text{Cr}_2\text{O}_3$ at all temperatures measured. So, the RC time constants for the electrochemical oxygen reactions at the electrodes were controlled by resistance in platinum and chromia electrodes whereas by the capacitance in the LSFCO electrode and the time constants were found to vary from a few seconds to milliseconds in the temperature range of $500\text{--}700^\circ\text{C}$. But the observed difference in the oxygen sensing response times, of the order of minutes, between the electrodes at temperatures 500°C and below reveals that the rate determining step is not the charge transfer process in these electrodes specifically in Pt and Cr_2O_3 at lower temperatures. The only other possible reaction step making the response time high is the surface diffusion of oxygen adsorbates, which is mainly influenced by the electrode microstructure.

Acknowledgements

This work was supported by CISM through NSF grant #EEC-9523358 and DOE (DE-FC26-03NT41615) program. The authors thank Joe Trimboli for preparing the platinum colloids.

References

- [1] C. Xia, M. Liu, Novel cathodes for low temperature solid oxide fuel cells, *Adv. Mater.* 14 (2002) 521–523.
- [2] E.L. Brosha, R. Mukundan, D.R. Brown, F.H. Garzon, J.H. Visser, M. Zanini, B. Zhou, E.M. Logothetis, CO/HC sensors based on thin films of LaCoO_3 and $\text{La}_{0.8}\text{Sr}_{0.2}\text{CoO}_{3-\delta}$ metal oxides, *Sens. Actuators B* 69 (2000) 171–182.
- [3] N. Miura, G. Lu, N. Yamazoe, High temperature potentiometric/amperometric NO_x sensors combining stabilized zirconia with mixed-metal oxide electrode, *Sens. Actuators B* 52 (1998) 169–178.
- [4] N. Miura, S. Zhuikov, T. Ono, M. Hasei, N. Yamazoe, Mixed potential type sensor using stabilized zirconia and ZnFe_2O_4 sensing electrode for NO_x detection at high temperature, *Sens. Actuators B* 83 (2002) 222–229.
- [5] N.F. Szabo, P.K. Dutta, Correlation of sensing behavior of mixed potential sensors with chemical and electrochemical properties of electrodes, *Solid State Ionics* 171 (3–4) (2004) 183–190.
- [6] S.P.S. Badwal, New electrode materials for low temperature oxygen sensors, *J. Electroanal. Chem.* 146 (1983) 425–429.
- [7] N.L. Robertson, J.N. Michaels, Oxygen exchange on platinum electrodes in zirconia cells: location of electrochemical reaction sites, *J. Electrochem. Soc.* 137 (1990) 129–135.
- [8] V. Stancovski, S. Sridhar, U.B. Pal, Thermodynamic stability and interfacial impedance of solid electrolyte cells with noble metal electrodes, *J. Electroceram.* 3 (3) (1999) 279–299.
- [9] B.C.H. Steele, J.-M. Bae, Properties of $\text{La}_{0.6}\text{Sr}_{0.4}\text{Co}_{0.2}\text{Fe}_{0.8}\text{O}_{3-x}$ (LSFC) double layer cathodes on gadolinium doped cerium oxide (CGO) electrolytes. II. Role of oxygen exchange and diffusion, *Solid State Ionics* 106 (1998) 255–261.
- [10] S.B. Adler, Mechanism and kinetics of oxygen reduction on porous $\text{La}_{1-x}\text{Sr}_x\text{CoO}_{3-\delta}$ electrodes, *Solid State Ionics* 111 (1998) 125–134.
- [11] A. Endo, H. Fukunaga, C. Wen, K. Yamada, Cathodic reaction mechanism of dense $\text{La}_{0.6}\text{Sr}_{0.4}\text{CoO}_3$ and $\text{La}_{0.81}\text{Sr}_{0.09}\text{MnO}_3$ electrodes for solid oxide fuel cells, *Solid State Ionics* 135 (2000) 353–358.
- [12] E.P. Murray, T. Tsai, S.A. Barnett, Oxygen transfer processes in $(\text{La,Sr})\text{MnO}_3/\text{Y}_2\text{O}_3$ stabilized ZrO_2 cathodes: an impedance spectroscopy study, *Solid State Ionics* 110 (1998) 235–243.
- [13] A. Ringuedé, J. Fouletier, Oxygen reaction on strontium doped lanthanum cobaltite dense electrodes at intermediate temperatures, *Solid State Ionics* 139 (2001) 167–177.
- [14] Y.L. Yang, C.L. Chen, S.Y. Chen, C.W. Chu, A.J. Jacobson, Impedance studies of oxygen exchange on dense thin film electrodes of $\text{La}_{0.5}\text{Sr}_{0.5}\text{CoO}_{3-\delta}$, *J. Electrochem. Soc.* 147 (2000) 4001–4007.
- [15] G.Ch. Kostoglouidis, Ch. Fükos, Properties of A-site deficient $\text{La}_{0.6}\text{Sr}_{0.4}\text{Co}_{0.2}\text{Fe}_{0.8}\text{O}_{3-\delta}$ based perovskite oxides, *Solid State Ionics* 126 (1999) 143–151.
- [16] C.C. Chen, M.M. Nasralla, H.U. Anderson, M.A. Alim, Impedance response of $\text{La}_{0.6}\text{Sr}_{0.4}\text{Co}_{0.2}\text{Fe}_{0.8}\text{O}_3$ based electrochemical cells, *J. Electrochem. Soc.* 142 (1995) 491–496.
- [17] E.P. Murray, M.J. Sever, S.A. Barnett, Electrochemical performance of $(\text{La,Sr})(\text{Co,Fe})\text{O}_3\text{--}(\text{Ce,Gd})\text{O}_3$ composite cathodes, *Solid State Ionics* 148 (2002) 27–34.
- [18] S.P. Jiang, A comparison of O_2 reduction reactions on porous $(\text{La,Sr})\text{MnO}_3$ and $(\text{La,Sr})(\text{Co,Fe})\text{O}_3$ electrodes, *Solid State Ionics* 146 (2002) 1–22.
- [19] A. Holt, P. Kofstad, Electrical conductivity and defect structure of Cr_2O_3 . II. Reduced temperatures ($< \sim 1000^\circ\text{C}$), *Solid State Ionics* 69 (1994) 137–143.
- [20] J. Trimboli, P.K. Dutta, Oxidation chemistry and electrical activity of Pt on titania: development of a novel zeolite-filter hydrocarbon sensor, *Sens. Actuators* 102 (1) (2004) 132–141.
- [21] R. Ramamoorthy, P.K. Dutta, S.A. Akbar, Oxygen sensors: materials, methods, designs and applications, *J. Mater. Sci.* 38 (2003) 4271–4282.
- [22] I.D. Raistrick, J.R. Macdonald, D.R. Franceschetti, in: J.R. Macdonald (Ed.), *Impedance Spectroscopy—Emphasizing Solid Materials and Systems*, John Wiley & Sons, New York, 1987, pp. 90–91.
- [23] P.R. Warburton, M.P. Pagano, R. Hoover, M. Logman, K. Crytzer, Y.J. Warburton, Amperometric gas sensor response times, *Anal. Chem.* 70 (1998) 998–1006.
- [24] O.J. Velle, T. Norby, P. Kofstad, The electrode system $\text{O}_2/\text{Pt}/\text{ZrO}_2\text{:}8\text{Y}_2\text{O}_3$ investigated by impedance spectroscopy, *Solid State Ionics* 47 (1991) 161–167.
- [25] H. Liu, M.M. Stack, S.B. Lyon, Reactive element effects on the ionic transport processes in Cr_2O_3 scales, *Solid State Ionics* 109 (1998) 247–257.
- [26] M. Sahibzada, S.J. Benson, R.A. Rudkin, J.A. Kilner, Pd-promoted $\text{La}_{0.6}\text{Sr}_{0.4}\text{Co}_{0.2}\text{Fe}_{0.8}\text{O}_3$ cathodes, *Solid State Ionics* 113–115 (1998) 285–290.
- [27] J.-M. Bae, B.C.H. Steele, Properties of $\text{La}_{0.6}\text{Sr}_{0.4}\text{Co}_{0.2}\text{Fe}_{0.8}\text{O}_{3-\delta}$ (LSFC) double layer cathodes on gadolinium doped cerium oxide (CGO) electrolytes. I. Role of SiO_2 , *Solid State Ionics* 106 (1998) 247–253.
- [28] J. Jamnik, J. Maier, Generalized equivalent circuits for mass and charge transport: chemical capacitance and its implications, *Phys. Chem. Chem. Phys.* 3 (2001) 1668–1678.
- [29] S.P. Yoon, S.W. Nam, J. Han, T.-H. Lim, S.-A. Hong, S.-H. Hyun, Effect of electrode microstructure on gas-phase diffusion in solid oxide fuel cells, *Solid State Ionics* 166 (2004) 1–11.